Molecular Physics, 2012
http://dx.doi.org/10.1080/00268976.2012.756126

Study of titanium adsorption on perfect and defected BC_3 nanotubes using density functional theory

Seifollah Jalili[a,b,*], Mojdeh Akhavan[b] and Jeremy Schofield[c]

[a]*Department of Chemistry, K. N. Toosi University of Technology, Tehran, Iran;* [b]*Computational Physical Sciences Research Laboratory, School of Nano-Science, Institute for Research in Fundamental Sciences (IPM), Tehran, Iran;* [c]*Chemical Physics Theory Group, Department of Chemistry, University of Toronto, Toronto, Ontario, Canada*

(*Received 1 September 2012; final version received 29 November 2012*)

Density functional theory calculations were used to study the titanium (Ti) adsorption on perfect and defected (4, 0) BC_3 nanotubes, considering Stone–Wales and vacancy defects. The binding energy values for these nanotubes were larger than the corresponding values for carbon nanotubes. The charge transfer from the Ti atom to nanotube was observed for all systems studied. The most exothermic binding process occurred for the Ti adsorption on a native V_B defect, which showed minimum structural deformation with respect to a perfect BC_3 tube. In the case of a nanotube with a reconstructed carbon vacancy, the adsorption of Ti generated a half-metallic anti-ferromagnet. The results obtained in this paper are relevant for spintronics and hydrogen adsorption applications.

Keywords: vacancy defect; Stone–Wales topological defect; electronic band structure; density of states; metal–nanotube interaction; half-metallic anti-ferromagnet

1. Introduction

Adsorption of functional groups, such as transition metal (TM) atoms on the surface of carbon nanotubes (CNTs) has a profound effect on their properties. TM–CNT interaction is an effective way for tuning the electronic properties of nanotubes (NTs) [1,2] and promises many potential applications, such as the fabrication of nanowires [3], low-resistance ohmic contacts for the use in field-effect transistors [4], metal-supported structures for catalysis [5], hydrogen adsorption media [6] and nanodevices [7]. Electron-beam evaporation experiments have shown that TMs, such as Ti, Ni and Pd, can form continuous coatings on the surface of CNTs [8]. First-principles calculations confirm that titanium (Ti) chains [9] or complex nanowires [10] can be achieved by coating the NTs with metal atoms. This transforms semiconducting NTs to metals by producing additional states in their band gap region.

The boron doping is believed to improve the binding strength of transition [11] or alkali metals [12] to NTs. The electron-deficient boron atoms increase the binding energy and lower the metal–metal interactions, thereby reducing the surface diffusion of metal atoms and metal coalescence on the surface of NTs. Theoretical studies indicate that the electron-deficient BC_3 NTs, in which the boron atoms are integrated in the NT structure, have a lower diffusion barrier and higher adsorption energy for Li atoms [13]. This has been attributed to the strong propensity of boron atoms to accept electrons from lithium and is even more obvious in the case of BC_3 NTs with topological defects [14].

On the other hand, intrinsic defects in the sidewall of NTs should be considered in computational studies, because they naturally occur in synthetic NTs and have a significant effect on the interaction of TM atoms with NTs and the electronic properties of the complexes formed. The presence of defects, especially vacancies with a net magnetic moment, is shown to increase the reactivity of NTs for TMs [15–20]. It is believed that defected NTs can strongly adsorb TM atoms and avoid the clustering on the surface of tubes [16,21].

In this paper, we have studied the interaction of a Ti atom with perfect and defected zigzag BC_3 NTs using density functional theory (DFT) calculations. Single carbon (V_C) and boron (V_B) vacancies, and Stone–Wales (SW) topological defects have been considered and the results have been compared with a defect-free BC_3 NT.

2. Computational methods

Spin-polarized DFT calculations were performed using plane-wave basis set and ultrasoft pseudopotentials [22], implemented in the Quantum ESPRESSO package [23]. The generalized gradient approximation (GGA) with the Perdew–Burke–Ernzerhof functional [24] was used using a plane-wave cut-off of 420 eV.

*Corresponding author. Email: sjalili@kntu.ac.ir

The BC_3 NT was made from a (8, 0) CNT by replacing appropriate carbon atoms with borons. Four unit cells were chosen along the tube axis to avoid the interaction between the defects and their one-dimensional (1D) periodic images. The resulting NT had a length of 17.08 Å and 128 atoms, of which 32 atoms were B. Since the unit cell of a BC_3 sheet is about four times larger than that of the graphene sheet, a (n, m) BC_3 NT has a diameter close to a ($2n$, $2m$) CNT [25]. Therefore, a (4, 0) BC_3-NT is obtained from a (8, 0) CNT. The NT was placed in a tetragonal supercell of 20 Å × 20 Å × 17.08 Å to simulate an infinitely long 1D periodic system. The empty spaces along the x and y directions were included to avoid interactions in the xy plane.

An SW topological defect was formed by rotating a bond in the NT by 90°. Four types of SW defects are possible, which are created by rotating an axial or slanted C–C or B–C bond. The most stable structure has been shown to be obtained from the rotation of an axial C–C bond [26]. Carbon (V_C) and boron (V_B) vacancies were created by removing one atom from the NT sidewall. There are a number of possible structural reconstructions for these 'native' vacancies, taking place in order to reduce the number of dangling bonds. Based on our previous work [26], six structures were chosen (perfect, SW, V_B, V_C, native-V_B and native-V_C) and a Ti atom was placed on different possible sites (above the various rings and their common bonds) on the surface of these NTs.

The Ti-adsorbed NTs were fully relaxed using the convergence threshold of 0.01 meV in energy and 0.005 eV/Å in force. The Brillouin zone was sampled using the gamma point for relaxation and a 1 × 1 × 7 Monkhorst-Pack [27] grid of k-points for the calculation of energy and other

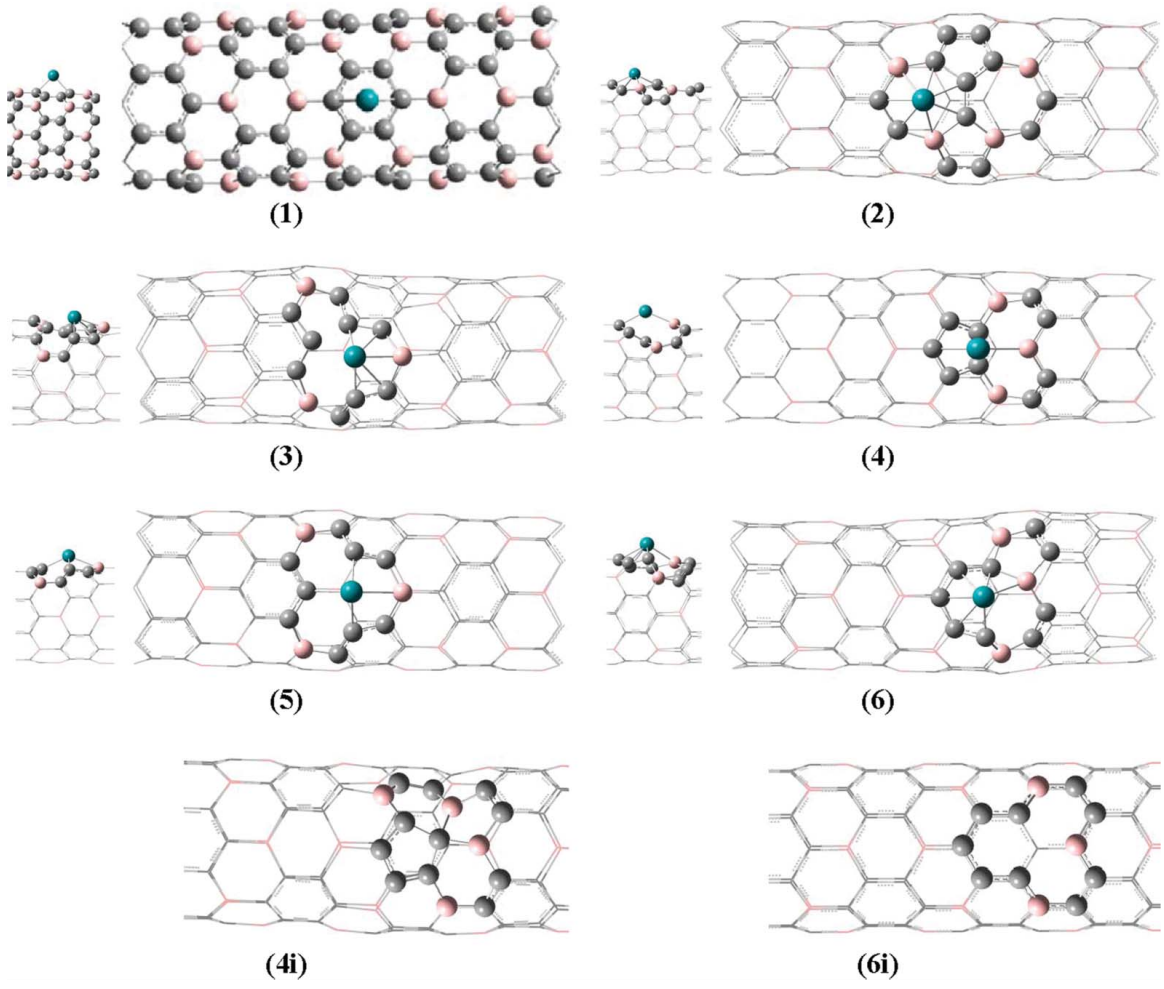

Figure 1. Optimized structures (top and side views) obtained for Ti-adsorbed perfect **(1)** and defected BC_3 nanotubes with a SW **(2)**, V_B **(3)**, V_C **(4)**, native V_B **(5)** and native V_C **(6)** defect. Initial structures for V_C **(4i)** and native V_C **(6i)** are also given.

Table 1. Properties of Ti-adsorbed BC_3 nanotubes. E_b^{sp} and E_b^{su} are binding energies obtained from spin-polarized and spin-unpolarized calculations, respectively. $d_{Ti\text{-}NT}$ is the average distance of Ti from neighbouring nanotube atoms, μ_B is the net magnetic moment and C is the charge transferred from the metal to nanotube.

System	E_b^{sp} (eV)	E_b^{su} (eV)	$d_{Ti\text{–}NT}$ (Å)	μ_B	C (e)
Perfect **(1)**	−4.40	−5.16	2.187	2.00	0.903
SW **(2)**	−5.28	−6.35	2.084	0.12	1.020
V_B **(3)**	−5.60	−6.93	2.132	1.00	0.936
V_C **(4)**	−4.46	−5.44	2.255	0.00	0.941
Native V_B **(5)**	−8.96	−10.11	2.153	1.00	0.958
Native V_C **(6)**	−8.42	−9.49	2.128	0.09	0.945

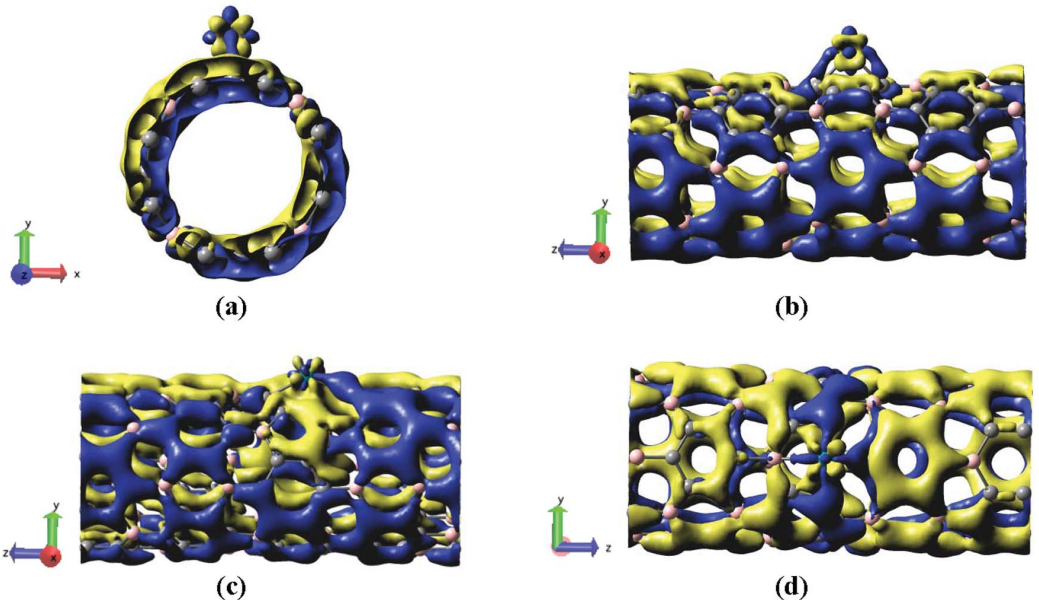

Figure 2. Charge density difference plots for Ti-adsorption on a perfect BC_3 tube from two views (a, b), a tube with V_C defect (c) and a tube with native V_B defect (d). Yellow (light) and blue (dark) regions correspond to charge depletion and accumulation, respectively.

properties. For band structure calculations, 11 k-points were chosen along the NT symmetry axis ΓZ.

The binding energy was calculated from $E_b = E(BC_3 - Ti) - E(BC_3) - E(Ti)$, where three energy terms are the total energy of fully optimized Ti-adsorbed NT, pure NT and the isolated Ti atom, respectively. All three terms were evaluated using a same supercell. A negative value for E_b corresponds to exothermic adsorption.

3. Results and discussion

Optimized structures for Ti-adsorbed BC_3 NTs are shown in Figure 1. Binding energies obtained from both spin-polarized (E_b^{sp}) and spin-unpolarized (E_b^{su}) calculations are given in Table 1. Generally, the absolute values of binding energies calculated from spin-relaxed structures are lower than the corresponding values from spin-unpolarized calculations, in accord with other works [1,2]. Table 1 also lists some of other properties such as net magnetic moments. Three out of six Ti-adsorbed BC_3 tubes are magnetic. The initial structures on which the Ti atoms were adsorbed have zero magnetic moments, unless the tubes with native V_B and V_C and reconstructed V_B defects (**3**, **5** and **6** in Figure 1) [26].

For a perfect BC_3 tube, the most favourable adsorption site for Ti is above a carbon hexagon (hollow site, **1** in Figure 1). A Ti atom makes bonds with two carbon atoms and its average distance from the carbons of neighbouring hexagon is 2.187 Å. The system has a magnetic moment of 2.00 μ_B (Table 1). These results are similar to the data obtained for Ti adsorption on a perfect (8, 0) CNT [1,2,21], but for the BC_3 tube, the binding energies are two times larger, since the electron-deficient boron atoms have greater affinity for metal atoms [12,13].

The most stable adsorption site on a BC_3 tube with SW defect is above a seven-membered ring, with an almost

zero magnetic moment (**2** in Figure 1). This agrees with the studies of Pt [28] and Cu [29] adsorption on CNTs with SW defects, but in the case of Ni and Ti adsorption on SW defects in a zigzag CNT, the (7,7) ring junction was shown to be the most favourable site [16,17,20,21]. In **2**, the Ti atom makes bonds with all atoms of the heptagon, and the average distance of Ti atom from the neighbouring NT atoms is lower than that of a perfect tube. The comparison of the binding energies given in Table 1 for **1** and **2** shows that Ti binds more favourably to a SW-defected BC_3 tube.

Structure **3** in Figure 1 shows the relaxed geometry for a Ti atom adsorbed on a NT with a single boron vacancy. The 'parallel' [26] orientation of the reconstructed (5,9) rings is maintained and the Ti atom is adsorbed above a part of these rings, making bonds with five atoms. The binding

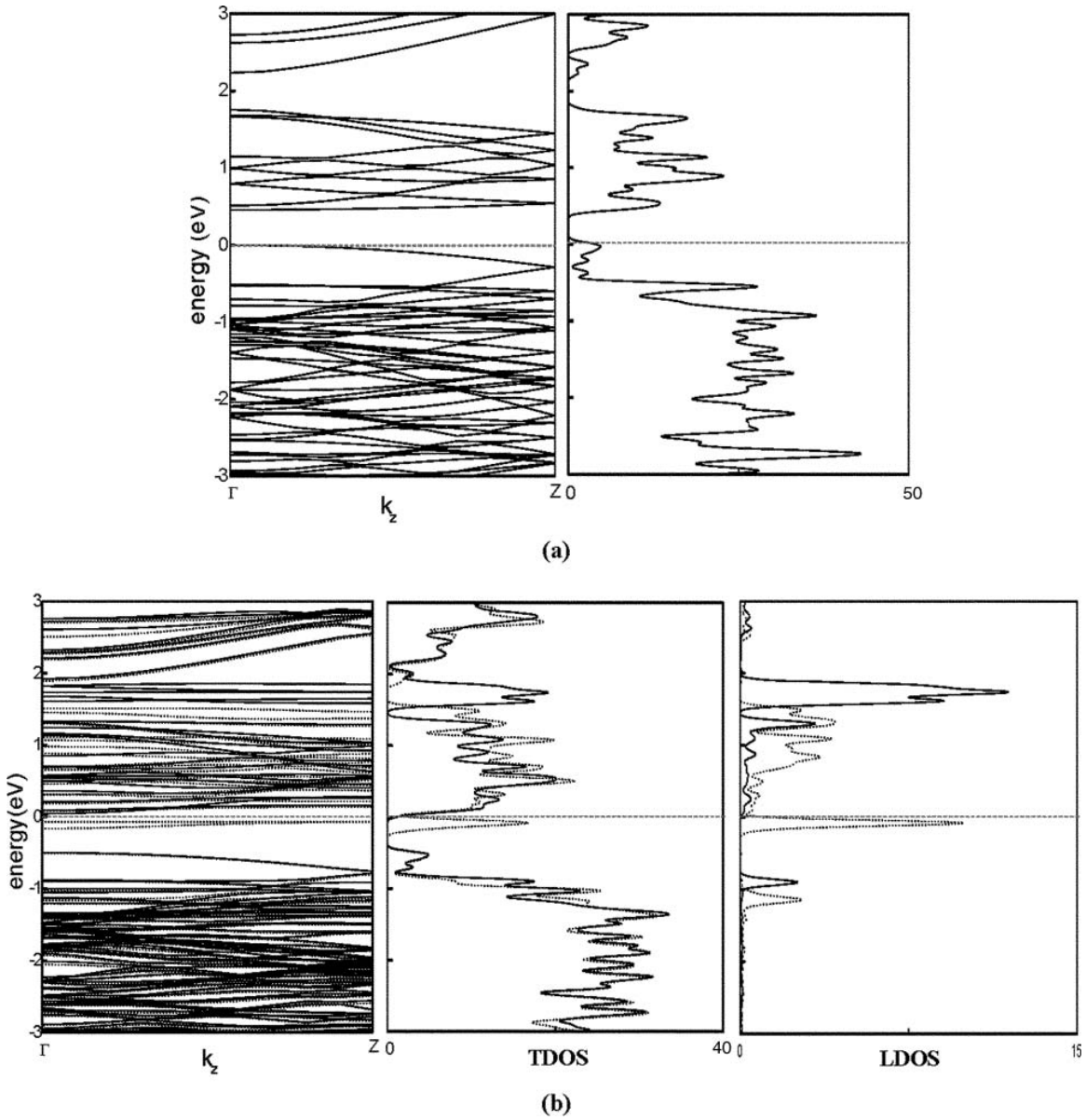

Figure 3. Electronic band structure and total and local (Ti) density of states for a perfect BC_3 nanotube without (a) and with (b) an adsorbed Ti atom. Spin-up and spin-down curves are shown by dotted and solid lines, respectively. The dashed line at zero energy indicates the position of the Fermi level.

energy is more negative than two preceding structures, indicating a better adsorption of Ti on a BC_3 tube with boron vacancy. The values of magnetic moments for **1**, **2** and **3** is inversely proportional to the number of bonds formed. It is noteworthy that the 'bonds' in Figure 1 are drawn simply based on a distance cut-off set-up in the GaussView programme [30].

The Ti adsorption on a BC_3 NT with a V_C defect changes its geometry from 'crossed' hexagon/pentagons (**4i** in Figure 1) [26] to a structure with 5- and 9-membered rings along the tube axis (**4** in Figure 1). The Ti atom adsorbs above the (5,9) junction, making bonds with two atoms. The net magnetic moment is 0, but its absolute value is 1.86 μ_B, which indicates an anti-ferromagnetic spin ordering. The absolute value of binding energy is slightly higher than that of a perfect BC_3 tube, but lower than the values for other defected tubes. In addition, this structure has the maximum metal-tube distance among the six systems studied. Based on energetic and structural data, this system is the least favourable one for the adsorption of Ti atoms.

The most negative values for the binding energy have been obtained for Ti adsorption above the native boron and carbon vacancies, i.e. the structures obtained from removing an atom from the NT surface, with three dangling bonds. In the case of native V_B (**5** in Figure 1), the Ti adsorbs with the minimum distortion in the original geometry and most negative binding energy. The metal makes bonds with four atoms around the defect site, with the average distance of 2.153 Å from neighbouring atoms. For the adsorption on native V_C defect (**6** in Figure 1), a reconstruction from the native defect (**6i**) to a 'parallel' geometry occurs, with a magnetic moment close to 0 and a binding energy that is slightly less negative than that of **6**. The local density approximation (LDA) and GGA calculations for the adsorption of Ti atom on a single vacancy in (8,0) CNT showed the binding energies of -8.02 and -9.23 eV, respectively [21].

Table 1 gives the amount of charge transferred (C) from the metal atom to the NT. This charge transfer makes the Ti atom positive and enhances the binding. Systems with larger C values are characterized by shorter chemical bonds. To explore the nature of metal–nanotube interactions, the charge density difference was calculated from

$$\Delta\rho(\mathbf{r}) = \rho(\mathrm{BC_3\text{-}Ti}) - \rho(\mathrm{BC_3}) - \rho(\mathrm{Ti}),$$

where the total charge densities for the relaxed BC_3-Ti and BC_3 systems, and isolated Ti atom are all calculated in the same supercell. The isosurfaces for the charged density difference are plotted in Figure 2. For Ti adsorption on perfect BC_3 tube, the charge density is depleted from the d_{xy} orbital of Ti atom into its d_{z^2} orbital, which interacts with the π orbitals on carbon atoms in NT (Figure 2(a,b)). This is known as the Dewar interaction [31], which has been also observed in the interaction of defect-free CNTs with Ti atoms [21] and in metal–diboride NTs [32]. Similar results have been obtained for the BC_3 NT with a SW defect (graphs not shown). For native V_B defect (**5** in Figure 1), the charge depletion is from a d_{yz} orbital (Figure 2(d)). For other NTs with vacancy defects, no Dewar interaction is observed and the charge depletion/accumulation involves a mixture of atomic orbitals. The graph for V_C defect (**4** in Figure 1) is shown in Figure 2(c) as a sample.

Electronic band structure and the total density of states (TDOS) for a perfect BC_3 NT (Figure 3(a)) shows that it is a semiconductor with a direct band gap of $\sim$0.5 eV. Upon Ti adsorption, the Fermi level shifts up to the conduction band and the BC_3 NT becomes a metal, with a non-zero DOS at Fermi level (Figure 3(b)). Two spin-up bands appear below the Fermi level, which are mainly contributed from the Ti atom, as clear from the local DOS (LDOS) plot for the adsorbed Ti atom in Figure 3(b). Other spin-up and spin-down states of Ti occur above the Fermi level. This unequal distribution of spin-up and spin-down states leads to a net magnetic moment of 2.00 μ_B in the Ti-adsorbed perfect BC_3 tube (Table 1). This is in qualitative agreement with the results for Ti adsorption on a (8, 0) CNT [1,2].

The DOS plots for the tube with a SW defect are shown in Figure 4. Compared to a perfect BC_3 tube (Figure 4(a)), the defected system has an additional state in the band gap that lowers the energy gap and is an acceptor state (Figure 4(b)). When a Ti atom is adsorbed on the SW defect (Figure 4(c)), the Fermi level shifts up and the empty (acceptor) state of the defected tube just above the valence

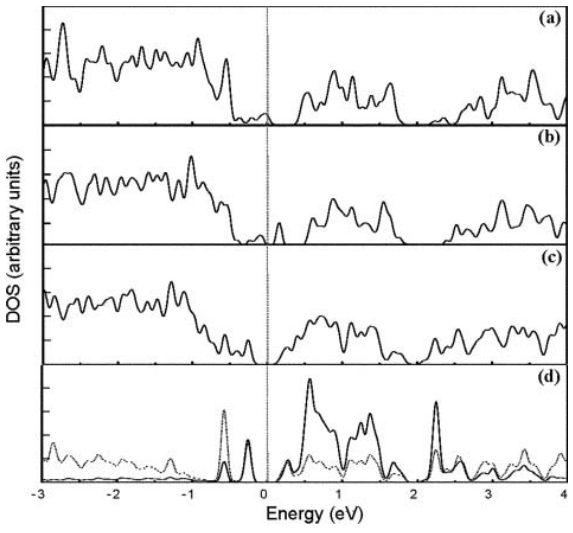

Figure 4. Total density of states for a perfect BC_3 tube (a), a BC_3 tube with a SW defect (b), a tube with SW defect and an adsorbed Ti atom (c) and local density of state plots (d) for Ti atom (solid line) and its neighbouring atoms in BC_3 tube (dotted line). The Fermi level is at zero energy.

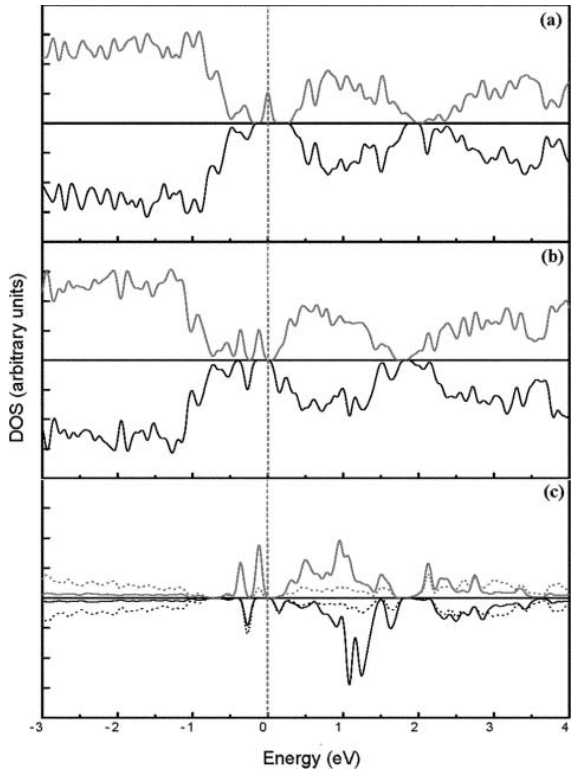

Figure 5. Total density of states for a tube with a V_B defect (a) and a tube with a V_B defect and an adsorbed Ti atom (b) and local density of states (c) for Ti atom (solid line) and its neighbouring atoms in BC_3 tube (dotted line). Upper and lower panels are for spin-up and spin-down states, respectively, and the Fermi level is at zero energy.

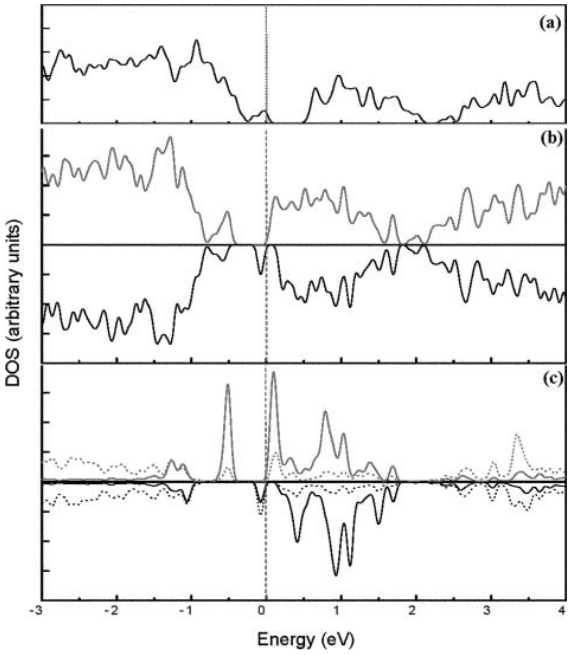

Figure 6. Total density of states for a tube with a V_C defect (a) and a tube with a V_C defect and an adsorbed Ti atom (b) and local density of states (c) for Ti atom (solid line) and its neighbouring atoms in BC_3 tube (dotted line). For the Ti-adsorbed tube, upper and lower panels are for spin-up and spin-down states, respectively, and the Fermi level is at zero energy.

band is now populated by Ti electrons and locates at the energy of -0.6 eV. In addition, a doubly occupied state appears at the energy of -0.3 eV, which is derived from the Ti atom states (Figure 4(d)). Other Ti states are formed in the conduction band. There is a band gap between the filled and empty states, which are derived from the Ti atom and have a significant contribution from the neighbouring atoms on NT, so this system is still a semiconductor.

Figure 5 shows the calculated TDOS and LDOS plots for the V_B defect. The defected BC_3 tube has a half-filled spin-up band at the Fermi level (Figure 5(a)), which upon the Ti adsorption is completely filled (Figures 5(b,c)). The Fermi level shifts up to the conduction band and two occupied states are formed below the Fermi level, which are occupied by two Ti electrons with opposite spins (Figure 5(c)). An additional spin-down empty state is formed just above the Fermi level, which has a contribution from the Ti atom and is derived from the tube states. The newly formed states improve the conductivity of the system.

For a BC_3 NT with a V_C defect, the structural deformation of NT upon Ti adsorption leads to considerable modification of the DOS plot. The Fermi level shifts up by a large value. The metal-free system is non-magnetic (Figure 6(a)), but after the Ti adsorption it shows different spin-up and spin-down DOS plots (Figure 6(b)), while the net magnetic moment of the system is 0. This is characteristic of half-metallic anti-ferromagnets [33,34], which are very important for spintronic applications [35]. New filled spin-down and empty spin-up states are formed near the Fermi level. The LDOS plots in Figure 6(c) show that these states are mainly contributed from the adatom, but the neighbouring atoms of Ti on BC_3 tube are important in the spin-down state below the Fermi level.

The band structure and total density of states for the Ti-adsorbed tubes with 'native' V_B and V_C defects are shown in Figure 7. The native-V_B defect adsorbs Ti and changes to a metal (Figure 7(a)). The LDOS plot in Figure 7(a) shows that the filled spin-up and empty spin-down bands near the Fermi level are mainly contributed from the Ti atom and its neighbouring NT atoms, respectively. By contrast, Figure 7(b) shows that in the Ti-adsorbed native-V_C defect, the system is non-magnetic and there is a small gap between filled and empty states below and above the Fermi level, which are mainly due to the adsorbed Ti atom.

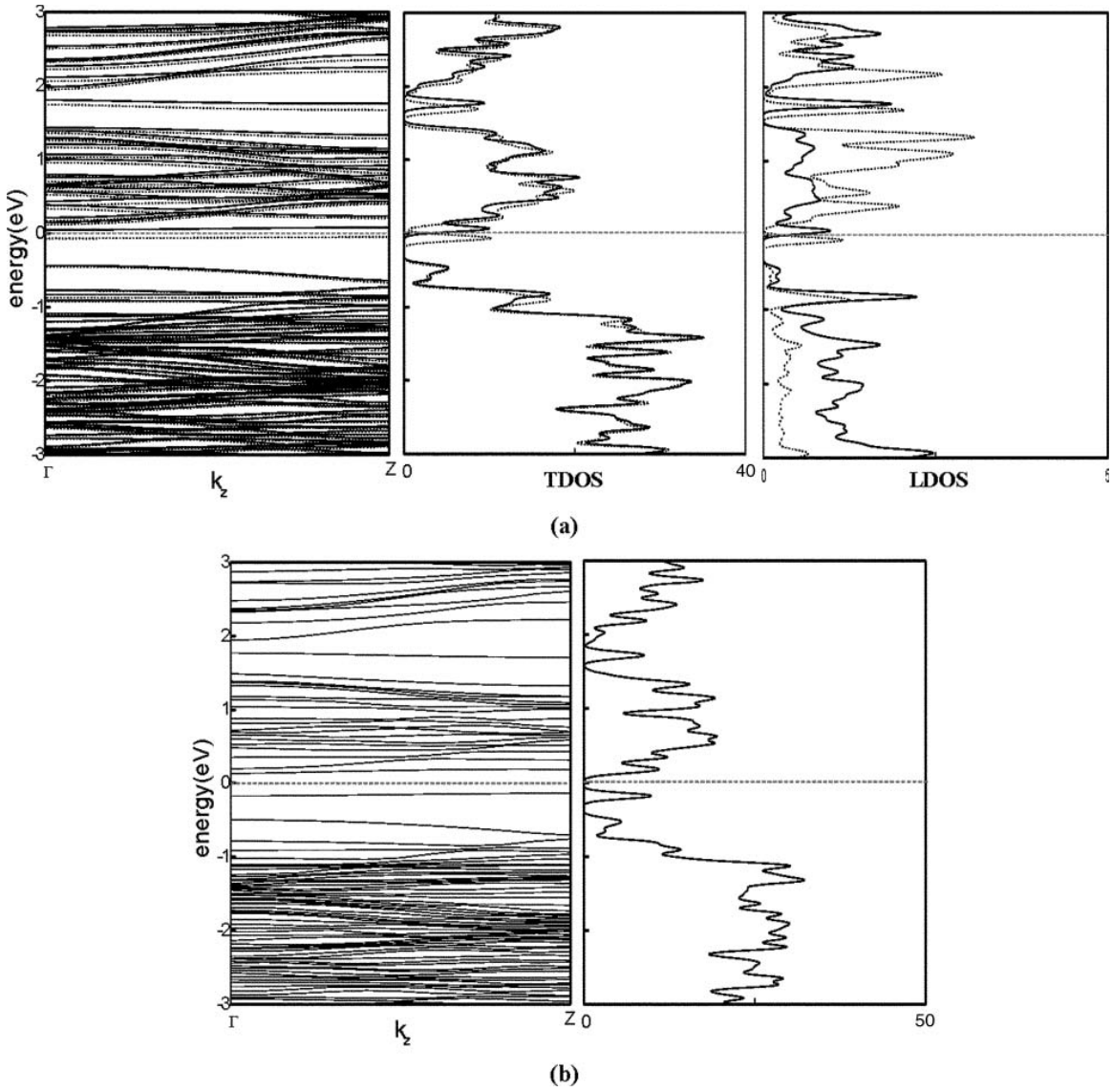

Figure 7. Electronic band structure and total and local density of states for Ti adsorption on a BC_3 tube with a native V_B (a) and a native V_C defect (b). Spin-up and spin-down curves are shown by dotted and solid lines, respectively. LDOS plot in part (a) is drawn for the spin-up states of Ti (dotted line) and spin-down states of neighbouring atoms in BC_3 tube (solid line). The dashed line at zero energy indicates the position of the Fermi level.

4. Conclusions

In the path to design novel nanomaterials with better Ti adsorption properties, we have chosen electron-deficient BC_3 NTs with different kinds of defects. The calculated binding energy values are generally larger than the values for corresponding CNTs. The most favourable systems on the basis of binding energy are BC_3 tubes with native vacancies, especially the native V_B defect, for which there is a little structural deformation in NT. This is a promising result, but it is necessary to perform additional calculations to test whether the coalescence of metal atoms occurs. For perfect and V_B-defected tubes, the Ti-adsorbed system has a net magnetic moment and shows metallic behaviour. For reconstructed V_C defect, the Ti adsorption leads to the half-metallic anti-ferromagnetic behaviour, which suggests a novel material with potential applications in spintronics.

Acknowledgements

This work has been supported by the Iran National Science Foundation (INSF). Computations were performed on the GPC supercomputer at the SciNet HPC Consortium. SciNet is funded by the Canada Foundation for Innovation under the auspices of Compute Canada; the Government of Ontario; Ontario Research Fund – Research Excellence; and the University of Toronto.

References

[1] E. Durgun, S. Dag, V.M.K. Bagci, O. Gülseren, T. Yildirim and S. Ciraci, Phys. Rev. B **67**, 201401 (2003).
[2] E. Durgun, S. Dag, S. Ciraci and O. Gülseren, J. Phys. Chem. B **108**, 575 (2004).
[3] E. Durgun and S. Ciraci, Phys. Rev. B **74**, 125404 (2006).
[4] C. Zhou, J. Kong and H. Dai, Appl. Phys. Lett. **76**, 1597 (2000).
[5] W. Li, C. Liang, W. Zhou, J. Qiu, Z. Zhou, G. Sun and Q. Xin, J. Phys. Chem. B **107**, 6292 (2003).
[6] T. Yildirim and S. Ciraci, Phys. Rev. Lett. **94**, 175501 (2005).
[7] Q. Zhao, M.B. Nardelli, W. Lu and J. Bernholc, Nano. Lett. **5**, 847 (2005).
[8] Y. Zhang, N.W. Franklin, R.J. Chen and H. Dai, Chem. Phys. Lett. **331**, 35 (2000).
[9] C.-K. Yang, J. Zhao and J.P. Lu, Phys. Rev. B **66**, 041403 (2002).
[10] S. Dag, E. Durgun and S. Ciraci, Phys. Rev. B **69**, 121407 (2004).
[11] Y. Zhao, Y.-H. Kim, A.C. Dillon, M.J. Heben and S.B. Zhang, Phys. Rev. Lett. **94**, 155504 (2005).
[12] Z. Zhou, X. Gao, J. Yan, D. Song and M. Morinaga, J. Phys. Chem. B **108**, 9023 (2004).
[13] Z. Zhou, J. Zhao, X. Gao, Z. Chen, J. Yan, P.v.R. Schleyer and M. Morinaga, Chem. Mater. **17**, 992 (2005).
[14] J. Zhao, B. Wen, Z. Zhou, Z. Chen and P.v.R. Schleyer, Chem. Phys. Lett. **415**, 323 (2005).
[15] H.S. Kim, H. Lee, K.S. Han, J.H. Kim, M.S. Song, M.S. Park, J.Y. Lee and J.K. Kang, J. Phys. Chem. B **109**, 8983 (2005).
[16] S.H. Yang, W.H. Shin and J.K. Kang, J. Chem. Phys. **125**, 084705 (2006).
[17] S.H. Yang, W.H. Shin, J.W. Lee, S.Y. Kim, S.I. Woo and J.K. Kang, J. Phys. Chem. B **110**, 13941 (2006).
[18] G.Y. Gou, B.C. Pan and L. Shi, J. Phys. Chem. C **112**, 13571 (2008).
[19] H.L. Zhuang, G.P. Zheng and A.K. Soh, Comput. Mater. Sci. **43**, 823 (2008).
[20] J.-X. Zhao and Y.-H. Ding, J. Phys. Chem. C **112**, 5778 (2008).
[21] S.A. Shevlin and Z.X. Guo, J. Phys. Chem. C **112**, 17456 (2008).
[22] D. Vanderbilt, Phys. Rev. B **41**, 7892 (1990).
[23] P. Giannozzi, S. Baroni, N. Bonini, M. Calandra, R. Car, C. Cavazzoni, D. Ceresoli, G.L. Chiarotti, M. Cococcioni, I. Dabo, A. Dal Corso, S. Fabris, G. Fratesi, S. de Gironcoli, R. Gebauer, U. Gerstmann, C. Gougoussis, A. Kokalj, M. Lazzeri, L. Martin-Samos, N. Marzari, F. Mauri, R. Mazzarello, S. Paolini, A. Pasquarello, L. Paulatto, C. Sbraccia, S. Scandolo, G. Sclauzero, A.P. Seitsonen, A. Smogunov, P. Umari and R.M. Wentzcovitch, J. Phys.: Condens. Matter **21**, 395502 (2009).
[24] J.P. Perdew, K. Burke and M. Ernzerhof, Phys. Rev. Lett. **77**, 3865 (1996).
[25] Y. Miyamoto, A. Rubio, S.G. Louie and M.L. Cohen, Phys. Rev. B **50**, 18360 (1994).
[26] S. Jalili, M. Akhavan and J. Schofield, J. Phys. Chem. C **116**, 13225 (2012).
[27] H.J. Monkhorst and J.D. Pack, Phys. Rev. B **13**, 5188 (1976).
[28] Y. Park, G. Kim and Y.H. Lee, Appl. Phys. Lett. **92**, 083108 (2008).
[29] C. Inntam and J. Limtrakul, J. Phys. Chem. C **114**, 21327 (2010).
[30] R. Dennington, T. Keith and J. Millam, *GaussView, Version 5* (Semichem Inc., Shawnee Mission, KS, 2009).
[31] D.M.P. Mingos, J. Organomet. Chem. **635**, 1 (2001).
[32] S. Meng, E. Kaxiras and Z. Zhang, Nano Lett. **7**, 663 (2007).
[33] H. van Leuken and R.A. de Groot, Phys. Rev. Lett. **74**, 1171 (1995).
[34] R.E. Rudd and W.E. Pickett, Phys. Rev. B **57**, 557 (1998).
[35] X. Hu, Adv. Mater. **24**, 294 (2012).